ECCOMAS Congress 2016
VII European Congress on Computational Methods in Applied Sciences and Engineering
M. Papadrakakis, V. Papadopoulos, G. Stefanou, V. Plevris (eds.)
Crete Island, Greece, 5–10 June 2016

GROUND TEST OF AN ENHANCED ADAPTIVE DROOP NOSE DEVICE

M. Kintscher[1], J. Kirn[2] and H.P. Monner[1]

[1]DLR Institute of Composite Structures and Adaptive Systems
Lilienthalplatz 7, 38108 Braunschweig, Germany
markus.kintscher@dlr.de

[2] Airbus Group Innovations, IC3 - Energy, Propulsion & Aerodynamics
81663 Munich, Germany
johannes.kirn@airbus.com

Keywords: Smart Droop Nose, Morphing, Leading Edge, High-Lift

Abstract. *For the application of laminar flow on commercial aircraft wings the high-lift devices at the leading edge play a major role. Since conventional leading edge devices like slats do not comply with the high surface quality requirements needed for laminar flow, alternative concepts must be developed. Besides the conventional Krueger device which enables laminar flow on the upper side of the airfoil and additionally implicates an insect shielding functionality, smart droop nose devices are currently under investigation. However, the research on such morphing devices which can deform to a given target shape and provide a smooth, high-quality surface has to give answers to questions of fundamental industrial requirements like erosion protection, anti/de-icing, lightning strike protection and bird strike protection. The integration of these functionalities into a given baseline-design of a morphing structure is a key challenge for the realization of such devices in the future. This paper focuses on the design drivers, system interdependencies and effects of the integration of the mentioned functionalities into a smart droop nose device developed in the European project SARISTU. The paper presents the concept and design procedure for the enhanced adaptive droop nose with focus on the integration of additional functionalities. It gives an overview on the functional demonstrators realized in the framework of the project and the setup and results of the large-scale ground test.*

1 Introduction

Because of the large potential of drag reduction natural laminar flow is one of the challenging aims of the current international aerospace research triggered by the ACARE research agendas [1, 2]. For the achievement of the absolutely essential high surface quality, new concepts for the high lift system at the leading edge are required. Besides the well-known Krueger device smart droop nose devices are investigated by various research facilities in Europe [3, 4, 5]. However, smart droop nose devices at the leading edge are not only advantageous for laminar flow wings. Applied at turbulent wings smart step- and gap less leading edge devices reduce the noise exposure in approach and landing as well as drag during take-off [6]. Already in 2007 the Institute of Composite Structures and Adaptive Systems at the German Aerospace Center (DLR) in cooperation with Airbus started a new morphing activity aiming at smart leading edge devices. In national and European projects the concept was consequently advanced and matured. It was successfully tested in a full-scale structural ground tests in 2010 [7] as well as in a full-scale low speed wind tunnel test [8] in 2012. In the ground test and in the wind tunnel test the feasibility of a load carrying smart droop nose device for a pre-defined aerodynamically optimized shape was successfully demonstrated. Since the work in recent projects was focused on the demonstration of feasibility of this technology, the integration of required technologies for the application at an aircrafts wing are investigated in the follow-up European project SARISTU (Smart Intelligent Aircraft Structures)[9]. This includes namely the integration of

- Anti/de-icing functionality
- Erosion protection
- Impact protection
- Bird strike protection and
- Lightning strike protection.

The participating project partners have been the Airbus Group Innovations for the design of the aero-mechanical kinematics and the erosion protection concept, INVENT GmbH for manufacturing of extreme lightweight fiber reinforced structures and prototypes, GKN Aerospace for the de-/anti-icing technology, SONACA as specialist for bird strike protection design, VZLU for manufacturing of the kinematic mechanism and bird strike tests as well as for carrying out the ground test of a full-scale leading edge section and finally the RWTH Aachen for the technology assessment on overall aircraft level. Emphasis in the project was on the integrational aspects of functionalities. Especially the effect of the additional functional layers or functions on the developed design procedure for design and sizing of smart leading edge devices was of interest. Furthermore, the design of a smart droop nose device in SARISTU is the first time focused on an outboard wing segment due to demonstration and testing activities of this full-scale outboard wing section in a wind tunnel test. The small design space and the large curvature at the leading edge tip of the airfoil combined with small chord length was additionally challenging for the design.

2 Concept, Design and Integration of Functional Layers

The chance of success of the integration of functional layers into shape adaptable structures strongly depends on the given boundary conditions and requirements. Furthermore the basic idea how to realize a shape adaptable leading edge is presented in the following chapters.

2.1 Concept and Design Procedure

A starting point for the structural concept for the design of the smart leading edge is the patent DE 2907912-A1 [10]. Following this patent the concept is based on a completely closed skin without any steps and slots and a comparably simple inner mechanism for actuation of the device (Fig. 1). The outer flexible skin is supported by a number of *omega*-stringers which act as longitudinal stiffeners and represent the attachment of the actuation mechanism at the same time. The inner mechanism is acting as an 'active' rib and is responsible for the deformation of the skin structure. It replaces the conventional nose rib. For sizing and optimization of the smart droop nose structure rethinking of the conventional design and sizing procedures is necessary. The design and optimization procedure developed in the previous projects had to be further developed to represent/take into account the strong interdependencies of the various seemingly contradictory functionalities. The design of the baseline flexible skin structure therefore depends strongly on other requirements like lightning strike protection as will be presented in the next chapters. However, for the design and sizing of the skin the applied design procedure has to consider the adverse requirements of morphing structures which are

- Large deformation but at minimum strain
- Stiff enough for high surface quality under aerodynamic loading but low actuator forces for the shape changing
- Load carrying inner kinematic mechanism for high surface quality but low complexity and weight.

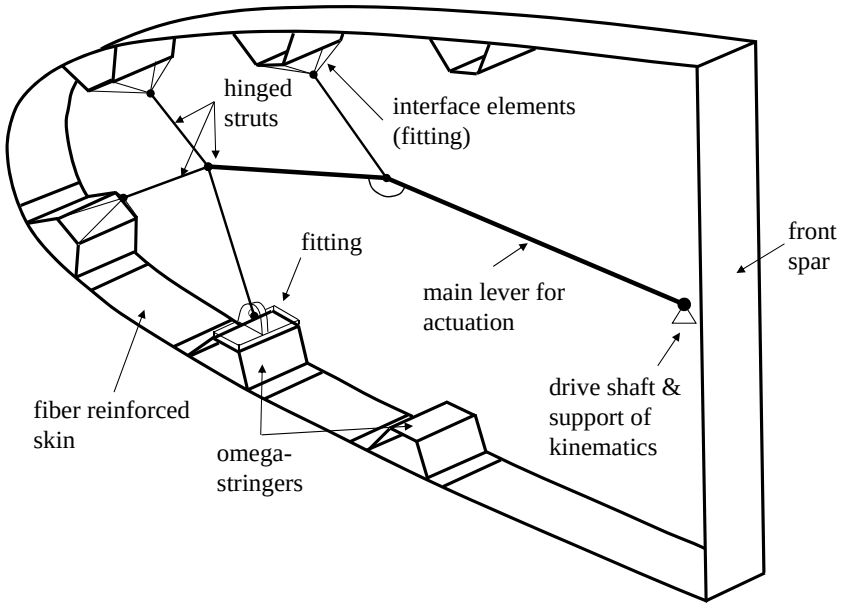

Figure 1: Conceptual design of a smart droop nose cross-section.

2.2 Wing Geometry and Ground Demonstrators

The targeted wing section is the outer wing of a business jet reference aircraft aiming at 130PAX. The overall main characteristic geometry relevant for the leading edge design is given

in Fig. 2 and Tab. 1.

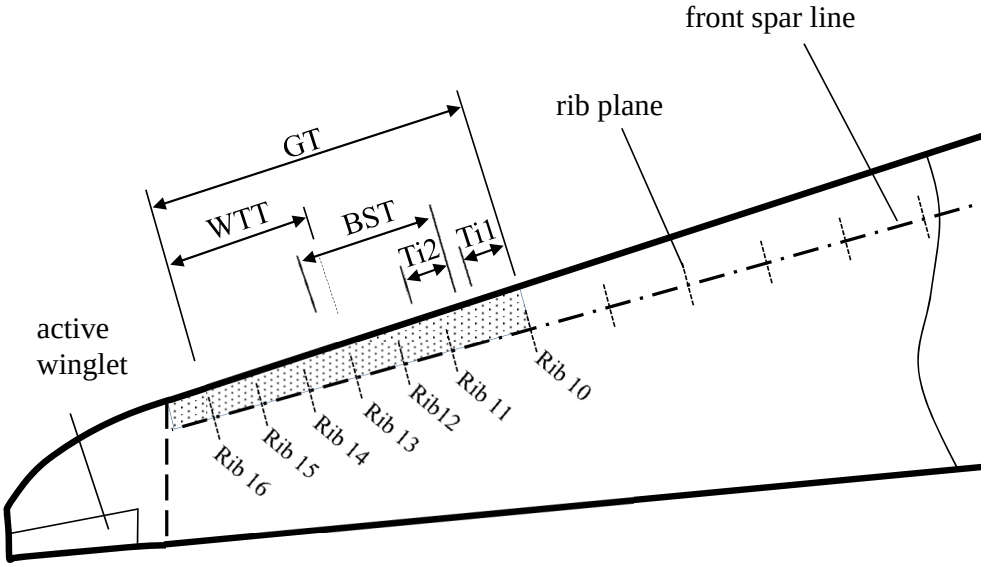

Figure 2: Overview of leading edge sections and test manufactured/performed in SARISTU.

In order to demonstrate the technology readiness level of the developed concept with regard to the various functionalities, several demonstrators have been realized within SARISTU. The objective of the ground test demonstrator (GT) is the investigation of wing bending and deployment of the leading edge in combination with an integrated heating device for de-icing. Of special interest are the effects on stress/strain and stability of the structural parts because of the state of a double curved structure when loaded. Moreover, a cyclic test is performed to identify components or locations which are prone to fatigue. The wind tunnel demonstrator (WTT) is tested in the T-104 wind tunnel at TsAGI Moscow up to a flow speed of about 120m/s. The objective here is the investigation of the structural deformation under relevant aerodynamic loading. In the Bird Strike Tests (BST) two different kind of bird splitters are tested. Since the morphing skin is relatively thin to allow for large deformations, bird strike protection is integrated by a standalone bird splitter structure. Besides a standard solid aluminum splitter a hybrid splitter made of aluminum sheets and an aluminum honeycomb core is tested. There have been two shots on the splitter structures without skin and one shot with a fully assembled leading edge section including skin and kinematics to check the effectiveness of the bird strike protection. As the erosion protection layer had not achieved a sufficient TRL level before the design freeze of the WT, GT and BST tests, it was omitted during these. For demonstration of the compatibility of the erosion protection layer there are two additional demonstrators (Ti1 & Ti2). These demonstrators are fully equipped short versions of the GT demonstrator with an additional titanium erosion shield, to demonstrate one possible approach for the integration of all required functional layers into shape adaptable/morphing structures.

2.3 Morphing Skin Design

Based on the patent [10] the developed structural concept in Fig. 1 features a flexible glass fiber structure as outer skin which is actuated by a conventional actuator and kinematic mechanism with regularly distributed stations in span direction. The glass fiber structure is especially

Acr.	Rib Station	Length	Test/Demonstrator	Topic
GT	Rib 10-Rib 16	3656mm	Wing Bending, fatigue, heater-mat	Shape, Strain, Strength
WTT	Rib 13-Rib 16	1760mm	aerodynamic loads	Shape, Strain
BST	Rib 11-Rib 12	1600mm	Bird Strike Test	Bird Strike Performance
Ti1	Rib 10	300mm	Ti-Foil (full-chord) and heater-mat	Shape
Ti2	Rib 11	300mm	Ti-Foil (patch)	Shape, Strain, Strength

Table 1: Overview of leading edge sections and test manufactured/performed in SARISTU.

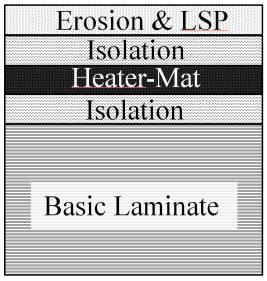

Figure 3: Schematic of skin stacking sequence with integrated functional layers.

tailored to achieve the desired aerodynamic target shape. The structure is fully closed in chord direction so that there are no steps and gaps and a high quality surface is guaranteed. The actuator forces are introduced into the skin structure by an inner kinematic mechanism which is attached to the skin using span wise oriented omega stringers as load introduction structure. The objective of the design procedure is a baseline GFRP skin which defines the carrying structure on which functional layers can then be applied. It is tailored for achieving a predefined target shape when actuated at a minimum of load introduction points. To reduce the strain in the GFRP skin when actuated, the design process is based on a certain design philosophy. This philosophy allows only bending of the structure when actuated without considering aerodynamic forces, so that membrane stresses and strains are avoided. This enlarges the allowable deformation, since the bending strain when deformed is not superimposed by membrane strain. By tailoring of the skins thickness the stiffness distribution (bending stiffness) is adapted in a way that

- a minimum of load introduction points is needed for actuation of the airfoil
- the stiffness is sufficient to carry the loads in cruise flight and provide a high quality surface
- the target shape when deployed can be provided considering the aerodynamic loads in take-off and landing).

This design philosophy allows for relaxation of the strain and large deformation of the airfoil since the leading edge represents a continuous geometry so that deformation and strain can be spread and evolve over the full available leading edge structure. The critical strains are observed at positions of large difference in curvature between undeformed and deformed shape of the leading edge in combination with the local skin thickness since the maximum bending strain ϵ_{Bmax} depends directly on the difference in curvature $\Delta\kappa$ and the thickness t of the skin

$$\epsilon_{Bmax} = \frac{1}{2}\Delta\kappa t. \tag{1}$$

Flexibility is provided by tapering the skin to a minimum skin thickness at locations of large difference in curvature between the undeformed and deformed shape of the structure. However,

the integrated functional layers in the stacking sequence lead to an unsymmetrical laminate (see sketch in Fig. 3).Therefore the neutral fiber of the laminate is shifted out of the symmetry plane of the laminates thickness. This effect is especially important to take into account in the design process especially if an erosion protection shield of a relative high stiffness compared to GFRP is applied. Since the standard materials applied for erosion protection are steel and titanium, this additional functional layer leads to an increased stiffness compared to the basic GFRP design. Furthermore these materials lead to a limitation of the maximum achievable difference in curvature due to their lower strain limits. Increasing the thickness of the whole laminate by integrating additional functional layers and the consequential shifting of the neutral fiber complicate the design furthermore.

2.4 Ground Test Finite Element Model

For the setup and planning of the experimental test a complete FE model of the test-rig including the leading edge skin structure, spars, kinematics and actuation is created (Fig. 4). For an efficient computation shell elements are used for the skin, omega-stringers, spars and flanges. For entities of the kinematic mechanism beam and Multi-Point-Constraints (MPC)-elements are used. To be able to simulate the full test program a priori to the test, the model is equipped with a fully functional drive shaft with actuation and kinematic mechanism including friction bearings at interface rib positions and kinematic flanges. This model will be validated with the experimental data of the large scale ground test.

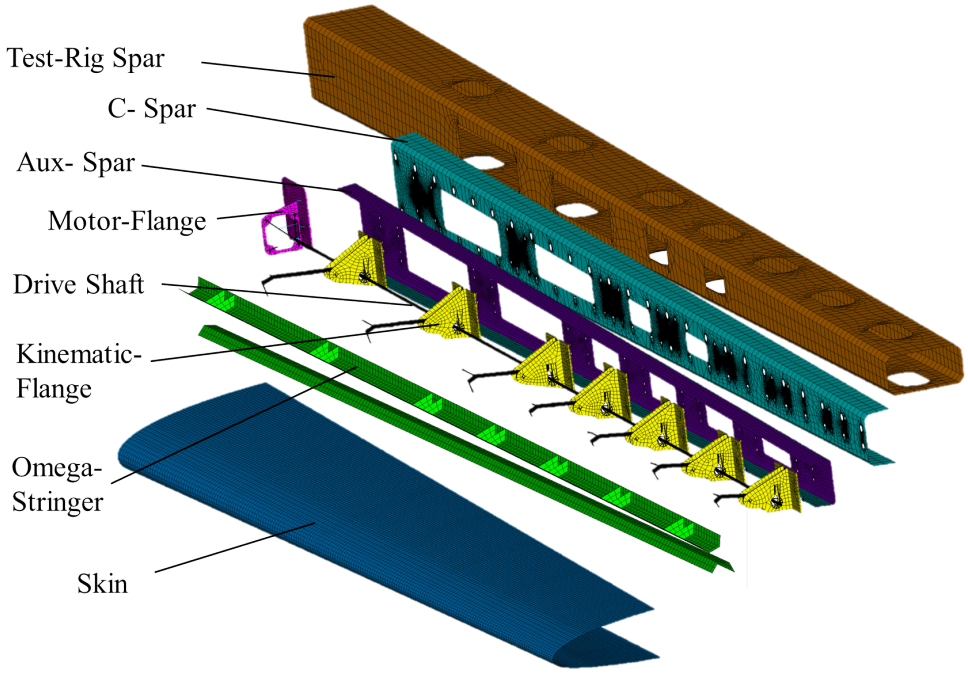

Figure 4: Finite element model of enhanced adaptive droop nose and test-rig assembly.

3 Experimental Ground Test

The main objective of the experimental tests is the demonstration of the functionality of the enhanced adaptive droop nose under relevant loading conditions. This includes wing bending

and cyclic fatigue. Additionally the identification of characteristic data like actuation force, strain and the demonstration of the capability of de-/anti- icing is important. The experimental data is used for the validation of the corresponding finite element models for the prediction of the structural behavior under various loading conditions and gives insight into the interaction of the various integrated functionalities and the structural reactions. A detailed description of the test setup, the objectives and the results is given in the following sections.

3.1 Ground Test Setup

The test setup is developed and realized with the contributing partners AGI and DLR under responsibility of VZLU. The test rig serves as an artificial front spar for the static as well as for the cyclic test of the smart leading edge. It consists of a massive spar made from steel which is supported at three stations in span by hydraulic load-cylinders for the application of wing bending forces to achieve a given wing bending line. Attached to the front spar is the leading edge structure which is pre-assembled to a thin aluminum spar. This pre-assembly is done for feasibility and handling reasons. The leading edge skin is bolted to the main front spar while the thin aluminum spar (called aux-spar in the following) is bolted to the front spar web. Inside of the leading edge the kinematic system is pre-installed which is then simply connected to the actuator which is attached to the rigid part of the test rig. An overview is given in Fig. 5.

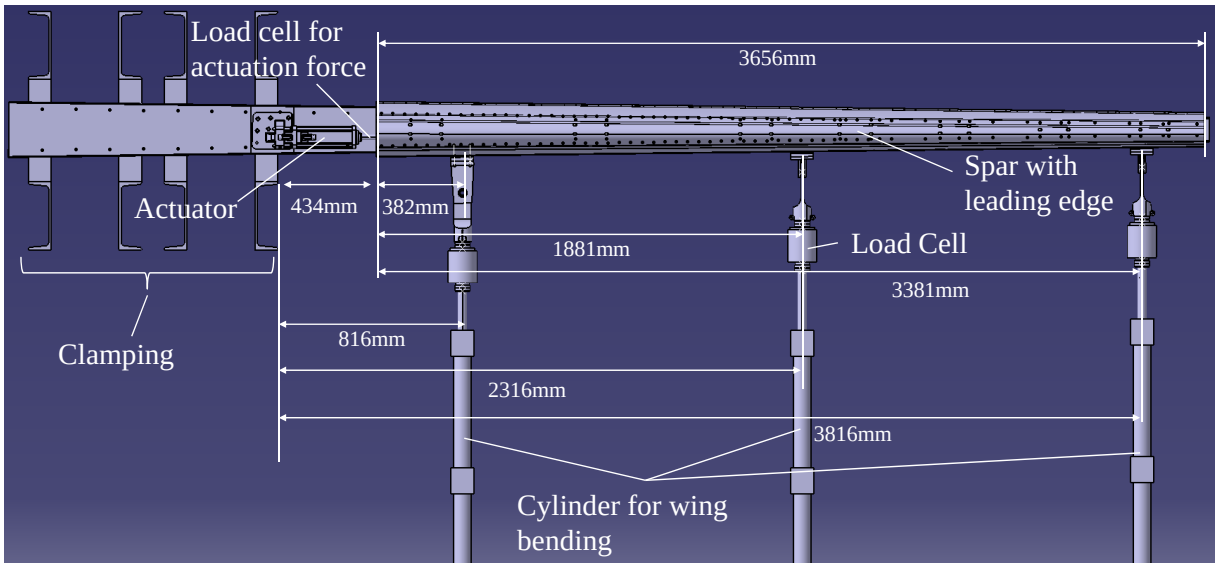

Figure 5: Test-rig setup for large ground test.

3.2 Instrumentation

For deformation measurements of the leading edge a GOM PONTOS System is used. PONTOS is a non-contact optical 3D measuring system. It analyses, computes and documents rigid body movements in discrete points with measured 3D positions. The measuring results can be graphically represented in reports using colored deviation vectors and/or diagrams. Two PONTOS cameras were situated on a stand. The camera sensors were calibrated before the measurements on the day of testing by using the calibration cross. The measuring volume for the available calibration cross and support was *1700mm x 1360mm x 1360mm*. The system was

able to measure one half of the leading edge at once. The two parts of the leading edge were measured separately for the same loading steps and then connected together using the PONTOS software and a CAD model of the leading edge. For on-line monitoring of the structural integrity and for comparison with FE calculation strains are monitored with standard strain gages. There are three strain gages for measurements of strains in chord direction on the outside of the skin structure each at every kinematic station number 10 to 16. For the measurement of strains in span direction there are four strain gages in chord direction (Fig. 6). The strain gage position is derived by FE calculations. For measuring the strains and forces acting on the kinematics various strain gages were positioned at critical locations. In total 12 strain gages, two angular sensors and one load cell were used to monitor the kinematic mechanism.

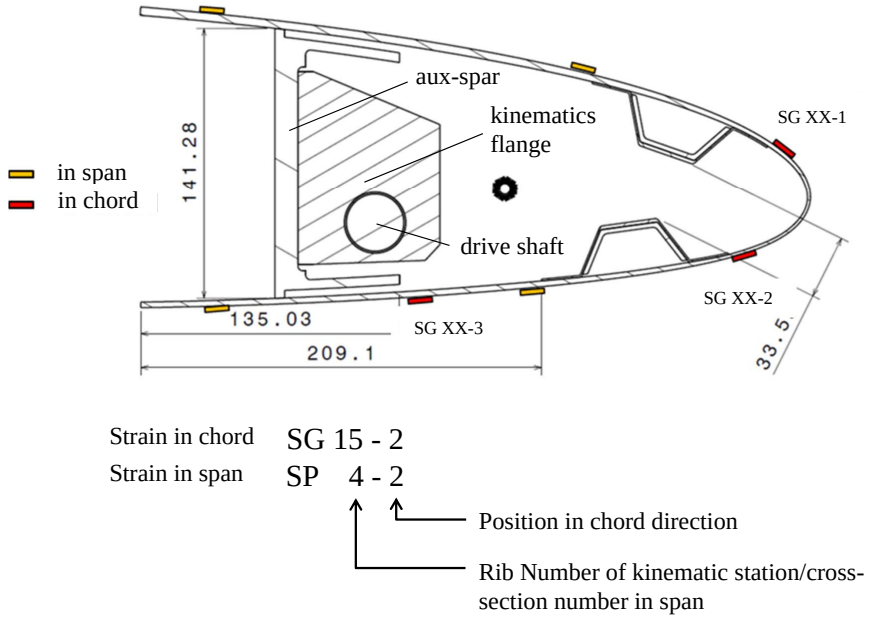

Figure 6: Nomenclature for applied strain gages.

The actuation force is measured by a load cell which is integrated directly after the actuator into the push-/pull- drive shaft mechanism (Fig. 5). The force for adjusting to the wing bending line is measured at every hydraulic cylinder by an integrated load cell. For monitoring of the heating system temperature sensors are applied as depicted in Fig. 7 in several heating zones and a FLIR thermal cam is used.

3.3 Results and Assessment

The results comparison for the structural ground test is done separately for the topics deformation, strain, forces and heater-mat performance for better overview.

3.3.1 Displacement & Shape

In Fig. 8 the comparison between predicted and measured leading edge displacements at maximum droop is presented. The prediction fits very well for the tip side of the leading edge. Larger deviations are observed on the inboard side. The negative difference at the inboard section means that the measured displacement was lower than predicted, with a relatively high

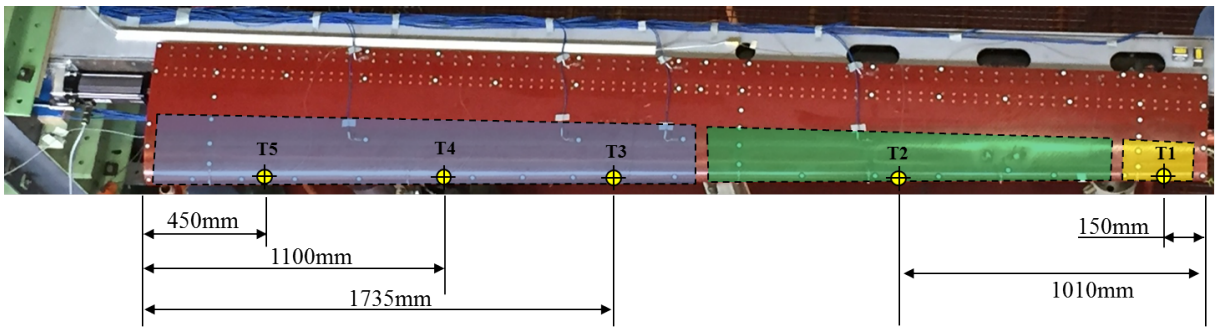

Figure 7: Position of thermo sensors and arrangement of heated leading edge sections.

difference of -12.5 mm i.e. up to -31% in this section. The result for the tip section indicates a small difference of 1 mm. The positive difference means that the real measured displacement was higher than predicted, up to 8% in this section. Compared to measurements in previous projects the difference at the inboard section are comparably large ($\pm 2mm$ in SADE-project [8]). The large difference inboards and inconsistency of the change in the middle of the leading edge is assumed to be caused by merging of two individual optical measurements for the respective sides. Due to the large size of data, unfortunately an on-line monitoring of the deformation data was not possible during the tests for immediate detection of this large difference. Unfortunately due to the limited testing time a repetition of the measurement was not possible to do after the test results assessment. However, the capability to design a leading edge structure for a given target shape was demonstrated in the SADE-project. The objective in the SARISTU ground test is the demonstration of the integration of additional functionalities for relevant load cases and deformations so that the exact approximation of a given target shape is of minor importance.

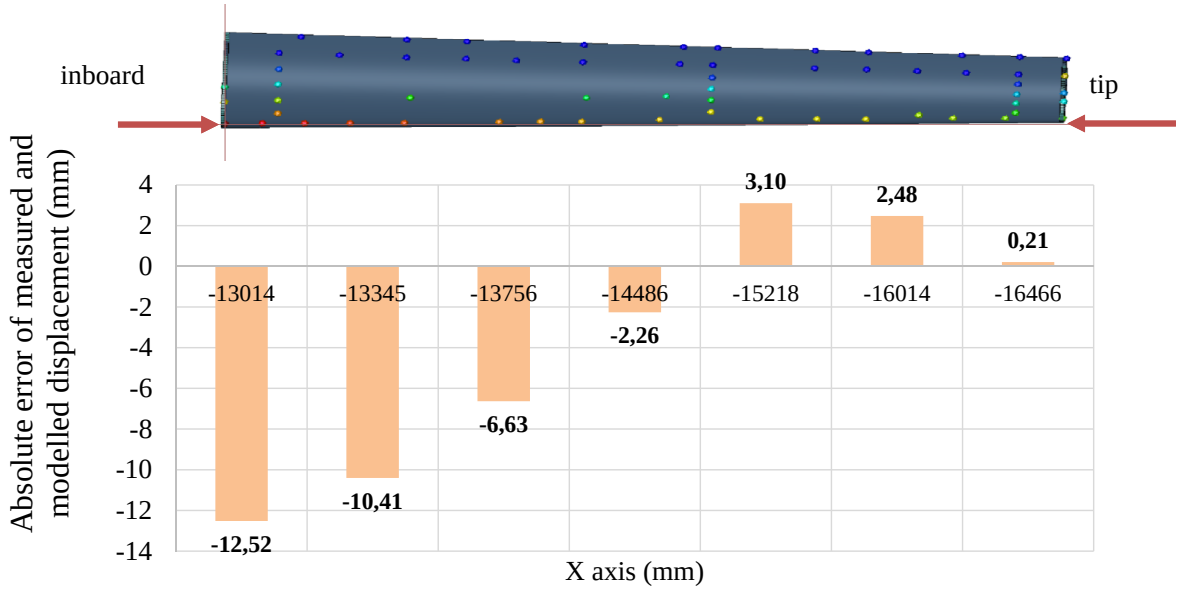

Figure 8: Absolute difference of measured and modeled displacements for leading edge.

3.3.2 Strain

In Fig. 9 the position of strain gages as well as the result from finite element analysis are given. The maximum strain considering wing bending and deployment of the leading edge is located at the lower side of the leading edge tip near the position of the integrated brackets for the attachment of the kinematics. Considering an additional layer of titanium on the outer surface for erosion protection for a two dimensional cross-section leads to the conclusion that the stress distribution changes considerably, namely a decrease in the outer layers and an increase in the inner layers of the GFRP. The maximum strain on the inside layers is dominated by the riveting line at the attachment to the spar. The maximum strain on the outside layers is dominated by the change in stiffness from stringer to skin as presented in Fig. 10. In the experimental measurements the maximum strain at the critical locations (SG xx-2) is in good agreement with the calculated strain values. A comparison with values from FEA for pure droop of the leading edge is given in Table 2.

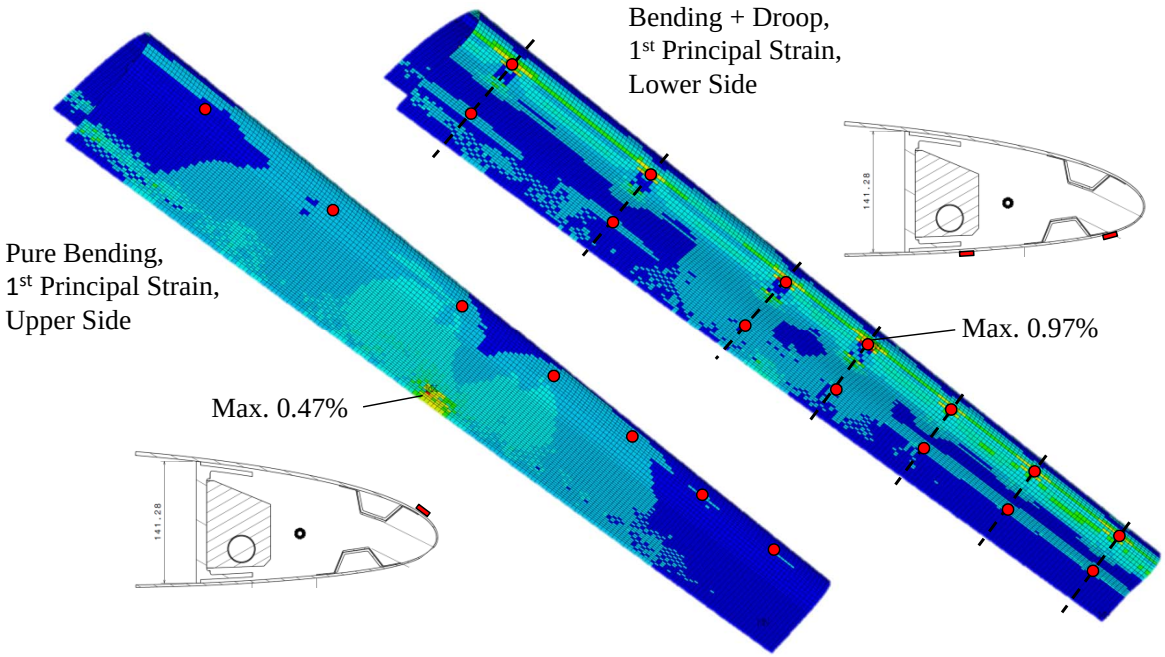

Figure 9: Position of strain gages and FE analysis of combined leading edge deployment (droop) and max. wing bending.

3.3.3 Forces

Comparing the measured maximum force of 6,7kN with the predicted actuator force (from FEA) shows a large discrepancy. FEA predicted a much lower maximum force. To measure the force during the test a HBM U9B load cell was used. Furthermore the progression of the force over time (see Fig. 11) reveals an unexpected behavior: The kinematic mechanism is designed for a zero force in fully deployed position since a toggle lever mechanism is used. However, in the force plot the force is increasing with reaching a minimum of about $-6700N$ (tension of the actuator) during deployment and then decreasing again. Finally in fully deployed position (at approx 14sec) it is stuck in a plateau. In this position the force is expected to be

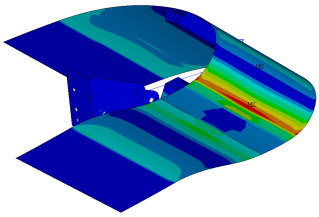

(a) Configuration with full-chord Ti, Layer 1, $\epsilon_{1,max} = 0.72\%$

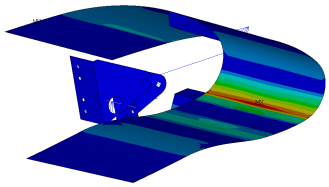

(b) Configuration without Ti, Layer 1, $\epsilon_{1,max} = 0.79\%$

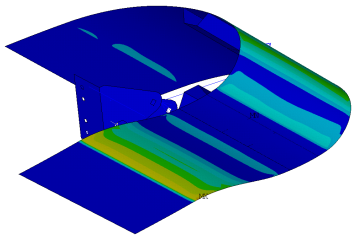

(c) Configuration with full-chord Ti, Layer 27, $\epsilon_{1,max} = 0.68\%$

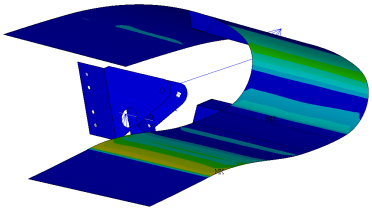

(d) Configuration without Ti, Layer 28, $\epsilon_{1,max} = 0.61\%$

Figure 10: Analysis of ϵ_1-strain distribution of titanium demonstrator (Ti1).

SG	$\epsilon_{1,max}$ in $\mu m/m$, *FEA*	$\epsilon_{1,max}$ in $\mu m/m$, *exper.*	Difference
SG 10-2	6400	6759	+5,6%
SG 11-2	6500	5771	-11,2%
SG 12-2	6800	7122	+4,7%
SG 13-2	7400	7723	+4,4%
SG 14-2	7150	8191	+15%
SG 15-2	8400	8792	+4,6%
SG 16-2	8577	8886	+3,6%

Table 2: Comparison of experimental and numerical maximum strains for pure droop (without wing bending).

zero. However, when starting to retract the leading edge (at 20sec.), the force immediately jumps to a positive value (compression of the drive shaft) then reaches a minimum and ends at zero. The effect is expected to be a combination of a tight tolerance setting of the actuator positioning system/controller and a non-linear sliding-friction/sticking-friction behavior due to the friction bearings in the rib flanges and the non-linear normal force resulting from the cross-link movement. Additionally the actuation angle is expected to be approx. $16.1°$ to $16.4°$ which does not agree with the measured $15.4°$ in the functional test. Since there was no time left for detailed investigations of this measurement deviation it is assumed to be an effect of the sensors sensitivity or misalignment at installation of the sensor.

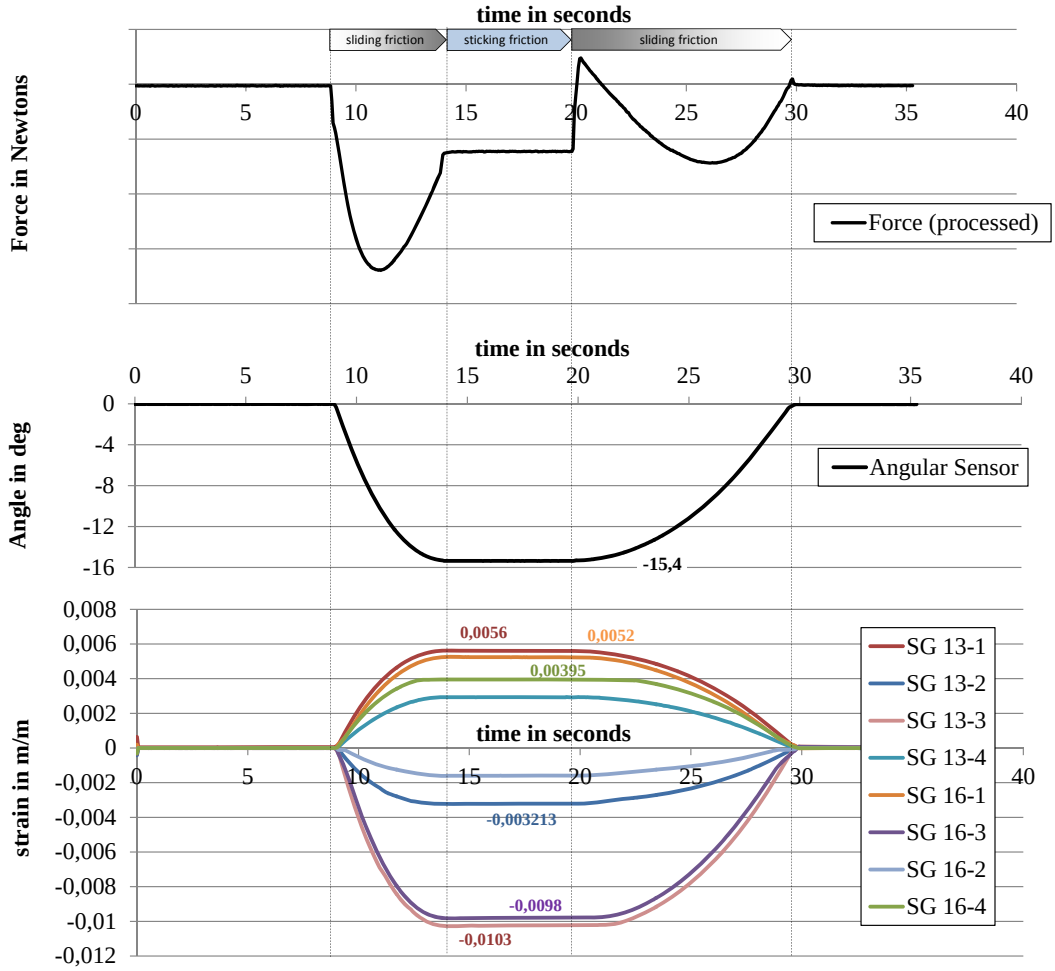

Figure 11: Test results of functional test of wind tunnel demonstrator (4 kinematic stations).

4 Conclusions

A challenge for morphing structure is the integration of essential functionalities for application at an aircraft. The successful integration of additional functionalities like de-icing, erosion protection and lightning strike protection was demonstrated by simulations, ground tests including wing bending and fatigue and a low speed wind tunnel test. The main challenge is the integration of additional functional layers without limiting the flexibility of the structure which is needed for relevant shape changing. Here a design has to consider the interdependencies of the partially adverse requirements of the functional layers to be integrated to find a balanced design. Depending on the applied material for the baseline skin structure the integration of additional functional layers (especially the comparably stiff erosion shield) causes a loss of predominance over the stiffness design of the structure. Since the adaptation of the shape is mainly steered by the difference in bending stiffness of the skin structure (which can be designed by tapering of the laminate layers), the more functional layers are integrated over the full leading edge chord length and the more stiff the integrated layers are, the less the shape can be adapted to a given aerodynamic shape. Furthermore, the achievable shape or deformation strongly depends on the maximum allowed strain of the various layers and materials of the functional layers. Additional functional layers in consequence mean an increased skin thickness which leads to

higher strains when the same difference in curvature is assumed. Furthermore, as the difference in curvature is increasing in span direction for a shape adaptation with constant parameters for the nose-down movement [1], the evolving strain increases not only with thickness but in span as well. This challenges the design for such a system at slim wings or at the outboard sections of a wing. Additionally, the available space is limited in outboard wing sections. Especially the auxiliary-spar concept for the attachment of the smart leading edge to the front spar turned out to have a decisive disadvantage: The attachment to the auxiliary spar as well as to the main spar needed a space of $130mm$ (constant over span) for riveting of the skin to both spars. At the outboard section this leads to a loss of about 9% of local chord length which cannot be used for realization of a specific design for the optimal aerodynamic shape. The realization of aerodynamically optimized shapes is therefore limited especially in the outboard sections of the wing. For large changes in curvature as needed on outboard wing sections new material combination like for example hybrid GFRP-elastomer skins as presented in [12] can be a better option. In general the integration of additional functional layers implies a reduction of layer thickness to the absolutely minimum in order to minimize the additional strain caused by the thickness of the skin structure. Special consideration is needed concerning the interdependency of lightning strike protection requirements and the heater-mat integration. The GFRP isolation layers which are separating the two functional layers increase the thickness of the skin and decrease the effectiveness of the heating system because of the thermal isolation. Using a material of high flexibility like titanium foil is mandatory for morphing structures. However the availability of thin titanium foil in large scale at the market is limited. Therefore other abrasion protection solutions like polyurethane protective tapes should be investigated.

REFERENCES

[1] ACARE, Vision 2020, European Commission.

[2] ACARE, Flightpath 2050, European Commission.

[3] A. De Gaspari and S. Ricci., Active Camber Morphing Wings Based on Compliant Structures, *Proceedings of the 2013 AIDAA Conference of the Italian Association of Aeronautics XXI Conference*, 9th 12th of September, 2013, Naples, Italy.

[4] D. Weber J. Mueller-Roemer, J. Simpson, S. Adachi, W. Herget, V. Landersheim, D. Laveuve, Smart Droop Nose for application to Laminar Wing of future Green Regional A/C. *Greener Aviation 2014*, 12.03.-14.03.2014, Brussels.

[5] G. A. A. Thuwis, M. M. Abdalla and Z. Guerdal, Optimization of a variable-stiffness skin for morphing high-lift devices, *Smart Materials and Structures, Vol. 19*, Number 124010, 2010.

[6] Wild, Jochen und Pott-Pollenske, Michael und Nagel, Bjoern, An integrated design approach for low noise exposing high-lift devices. *3rd AIAA Flow Control Conference*, 2006-06-05 - 2006-06-08, San Francisco, CA (USA).

[1] Shapes have been generated with the droop nose shape generator of T. Kuehn and J. Wild from [11]. Constant parameter is for example the droop in percentage of the local chord length.

[7] Monner, H. P., Riemenschneider, J. and Kintscher, M, Groundtest of a Composite Smart Droop Nose. *AIAA/ASMR/ASCE/AHS/ASC 2012*, 23.-26.04.2012, Honolulu, Hawaii. ISBN 10.2514/6.2012-1580.

[8] Kintscher, Markus und Monner, Hans Peter und Kuehn, T. und Wild, J., Wiedemann, Martin. Low speed wind tunnel test of a morphing leading edge, *Proceedings of the 2013 AIDAA Conference of the Italian Association of Aeronautics XXI Conference*, 9th 12th of September, 2013, Naples, Italy.

[9] SARISTU, FP7 project-consortium, http://www.saristu.eu

[10] H. Zimmer, Quertriebskoerper mit veraenderbarer Profilierung, insbesondere Flugzeugfluegel, German Patent No. DE 2907912-A1, 1979.

[11] Kuehn, T. und Wild, J.: Aerodynamic Optimization of a Two-Dimensional Two-Element High Lift Airfoil with a Smart Droop Nose Device. *1st EASN Association Workshop on Aerostructures*, 07.10.2010 - 08.10.2010, Paris, France, 2010.

[12] Schmitz, A. und Horst, P. und Rudenko, Anton und Monner, Hans Peter, Design of a contourvariable droop nose, *Forschungsbericht 2013-03, TU Braunschweig*, Techn. Univ., Campus Forschungsflughafen. Seiten 110-121. ISBN 978-3-928628-63-1.